

**Star Formation and Metal Production as a Function of Redshift:
The Role of the Multi-Phase ISM**

Marco Spaans and C. Marcella Carollo¹

Department of Physics & Astronomy, The Johns Hopkins University, Baltimore, MD 21218

Received _____; accepted _____

arXiv:astro-ph/9703109v2 18 Mar 1997

¹Hubble Fellow

ABSTRACT

We present models of the cosmological star formation and metal production history of (proto-)galaxies with varying axis ratios. More massive and/or roughly spherical systems reach the threshold-metallicity for a transition to a multi-phase interstellar medium earlier than less massive, more flattened systems. Therefore, more flattened, lower-mass systems start to form stars actively at smaller redshifts. A natural explanation is found in the overall robustness of the interstellar medium against complete expulsion (blow-away) at high total masses, and in the prevention of metal enrichment in the outer regions due to axial outflow along the symmetry axis of a non-spherical proto-galaxy (blow-out). We suggest that the observed predominance of spheroidal systems observed at high redshift, e.g. in the Hubble Deep Field, is due to this effect: At $z > 2$, roundish (proto-)galaxies with total (dark+baryonic) masses of $\approx 10^{11} M_{\odot}$ and/or the inner spheroidal cores of similarly massive flattened systems sustain a multi-phase interstellar medium, and therefore a high star-formation rate, whose magnitude depends on the fraction of baryonic matter in the systems. Conversely, the peak at $z \sim 1 - 2$ in the observed cosmological metal production rate coincides with the epochs of star formation of lower mass spheroidals, as well as of massive proto-galactic disks.

subject headings: cosmology: theory - galaxies: formation - galaxies: evolution - ISM - molecular processes

1. Introduction

The Hubble Deep Field (HDF; Williams et al. 1996) WFPC2 images and recent Keck spectroscopic data (Steidel et al. 1996, hereafter S96) indicate the presence of a population of star-forming galaxies at redshifts as high as ≈ 3.5 . Furthermore, the HST images indicate a narrow dispersion in morphological properties, in contrast to the variety found in star-forming galaxies at intermediate redshifts ($z \simeq 1$). The galaxies at high redshifts have a compact morphology, and are typically characterized by a small but resolved spheroidal core, often surrounded by lower surface brightness nebulosities (Giavalisco et al. 1996a, hereafter G96). The sizes and scale lengths of these cores are similar to those of present day bulges (G96). In contrast, galaxies at intermediate redshifts show a large variety of morphologies such as very irregular objects, systems with super-luminous star forming regions, and centrally located bright nuclei embedded in elongated or irregular faint nebulosities (c.f. Giavalisco et al. 1996b). The physical characteristics of the objects at high redshift are a subject of much debate. The interpretations range from merging sub-galactic clumps (Lowenthal et al., astro-ph/9612239) to massive disks (Prochaska & Wolfe 1997), or massive spheroidals (Pettini et al. 1994).

At the various redshifts, the physical structure of the Inter Stellar Medium (ISM) allows the formation of stars. Feedback mechanisms such as energy input from supernovas into the ISM, heating due to ionizing radiation, and stellar winds, play a fundamental role in regulating the formation of stars, and therefore in the production of metals. Madau et al. (1996, hereafter M96) have made an important step towards probing and understanding the metal history of the universe. These authors have shown that the metal production rate, which is a direct measure of the star formation rate, peaks at a redshift between 1 and 2. A first approach in understanding the cosmic chemical evolution with closed-box, inflow and outflow models has been presented by Fall (1996; see also Pei & Fall 1995).

The conditions necessary for the formation of a stellar population involve the ability to cool interstellar gas and form dense molecular clouds. Norman & Spaans (1997, NS97) and Spaans & Norman (1997, SN97) have suggested that the efficient formation of stars begins with a phase transition to a multi-phase ISM after a period of slow star formation regulated by H_2 cooling. This phase transition was computed to occur at a metallicity $\sim 0.01Z_\odot$ depending on the local star formation rate during this moderate phase. (NS97). Furthermore, an optimal metallicity range of $\sim 0.01 - 0.1Z_\odot$ was identified, for which star formation can proceed very efficiently (SN97). This result is independent of geometry and is due to the absence of magnetic support for the molecular clouds, because a low ionization fraction yields an ambipolar diffusion time scale shorter than the free-fall time of a molecular cloud. The opposite occurs at metallicities larger than $\sim 0.1Z_\odot$, and hampers the collapse of dense clouds and therefore the formation of stars. The optimal metallicity range can allow the occurrence of starbursts, which can have a dramatic effect on the evolution of dwarf galaxies, and in general leads to a period of intense star formation in more massive systems (SN97, NS97). For a general population of proto-galactic disks, the peak in star formation lies between $z = 1.2$ and 2 (NS97).

The apparent evolution with redshift of galaxy morphology observed in the deep imaging searches, and the observed redshift evolution of the metal formation rate in the universe, must be strongly related to the local physics of the multi-phase ISM. At each epoch, the ambient interstellar gas of systems forming stars with a high efficiency, must have a multi-phase structure with dense molecular clouds. As such, it appears timely to investigate the influence of geometry and mass on the occurrence of the transition to a multi-phase ISM, and on the star formation history of the luminous galaxies at intermediate to high redshifts.

2. The Model

The adopted model is described in detail in NS97 and SN97. Its basic ingredients are:

(1) The effects of feedback on the energy budget of the interstellar gas, due to the formation of stars and the occurrence of supernova explosions, are included explicitly and allow the self-consistent computation of the local star formation history. A Salpeter (1955) Initial Mass Function (IMF) is assumed. A modified Schmidt law, which includes the effects of ambipolar diffusion derived from the ionization balance in the ambient medium, is adopted to compute the local star formation rate. The total amount of energy injected into the ISM by supernova blast waves is used to compute the ejection rate of enriched interstellar gas.

(2) Prior to the phase transition, regions where the H_2 abundance is large are characterized by a kinetic temperature of ~ 1000 K due to vibrational line cooling (NS97). For each mass M and at each redshift z , the multi-phase structure of the ISM is calculated as a function of the ambient metallicity and of position in the galaxy. That is, given the local gravitational pressure, the equation of thermal balance is solved and its solutions used to determine the density and temperature of the cold and dense, and warm and ionized, medium.

(3) The loss of enriched interstellar material in non-spherical systems due to blow out along the short axis of the system is taken into account. The investigations of De Young & Heckman (1994) indicate that galaxies with masses $\geq 10^{11} M_\odot$ are robust against complete ISM expulsion caused by the pressure wave produced by SN explosions (blow-away). This result is independent of geometry, unless the stellar energy depositions are in excess of 10^{59} erg during a starburst phase. In flattened systems, this process leaves the outskirts of the ISM undisturbed, because the rarefaction wave produced by blow-out along the symmetry axis of the galaxy will overtake the expansion front (Figure 1 of De Young & Heckman

1994). That is, as the pressure driving the expansion front drops, the bubble of metal-rich hot gas stops expanding once its momentum is dissipated. An important consequence is that the spherical geometry allows the metal-rich gas to travel a longer distance through the galaxy than in the flattened case of similar mass, and leads to a faster enrichment.

Our models do not incorporate effects such as a varying IMF, or differential rotation. Biasing the IMF toward more massive stars alters the enrichment history of the ambient medium, and the relative abundance of the α versus iron-peak elements. Differential rotation might lead to a lower effective star-formation rate in the inner regions of galaxies, due to shearing of molecular clouds (as e.g., in our own Galaxy).

In this Letter we study in detail the star formation history of (proto-)galaxies with various geometries for the baryonic gas component, and different values of the total (dark+baryonic) mass. We consider oblate ellipsoidal systems with a baryonic mass of 5×10^{10} and $5 \times 10^{11} M_{\odot}$ and a radius of $\ell = (x^2 + y^2)^{1/2} = 8$ and 15 kpc, respectively, with axis ratios ranging from 1 (spherical geometry) to 0.6 (morphological type “E4”). The baryonic density profile is assumed to be $\rho \propto r^{-2}$, with $r^2 = x^2 + y^2 + qz^2$ and q the axis ratio, outside a 1 kpc constant density core. Constant baryonic to non-baryonic mass ratios of 0.2 and 0.04 are considered. Our models are intended to investigate the process of star formation in objects which sample the mass distribution provided by scenarios of hierarchical structure formation, but do not assume any specific prescription for it. However, the masses and redshifts that we investigate are consistent with standard CDM (see e.g., Figure 1 of NS97).

It is important to note that in massive galaxies the geometry-induced blow-out discussed in (4) occurs at an epoch when the outskirts have not been enriched yet. The blow-out phenomenon depends little on the (poorly known) shape of the dark matter halo for a fixed baryonic to non-baryonic mass ratio, given that the halos are more extended

than the baryonic matter, and is driven instead by the geometrical shape of the baryonic mass distribution. The time scale on which blown-out gas can be re-accreted depends on the total binding energy, i.e. the total (dark+baryonic) amount of matter present in the galaxy. Typical time scales are of the order of ~ 1 Gyr, and therefore this effect is not likely to alter the conclusions of our work.

The spheroidal systems studied in this work are associated with roughly spherically symmetric initial density perturbations which are turning around and are collapsing under the influence of gravity. As such, these systems are in quasi-equilibrium; the baryonic matter is partially pressure supported as it settles into the dark matter halo potential. Small deviations from sphericity will be amplified by gravitational collapse on a free-fall time (Cole & Lacey 1996). It is therefore expected that a range of geometries exists for the baryonic matter component. Any amount of non-zero angular momentum of the spheroidals, and changes in their original shape due to contraction, are ignored in our treatment of the local physics of star formation. Our simulations do not imply the formation of the Hubble sequence, nor do they require the formation of specific morphologies at specific redshifts. Instead our simulations will show how the physical structure of the ISM as a function of redshift, and therefore the star formation rate in the system, depends on the total mass, and on the morphology of the baryonic matter.

The time scales involved in the model are the following. The (proto-)galactic systems discussed above form on a free-fall time of ~ 1 Gyr due to cooling by Bremsstrahlung. During this time, only a small fraction of baryonic matter is converted into stars due to H_2 cooling (NS97). Supernova bubbles produced in the dense central regions expand on a time scale of ~ 20 Myr, and blow-out in flattened systems. The latter time scale is shorter than the time required to condense the metal-rich tenuous gas inside the expanding bubbles into dense molecular clouds in the presence of star formation (~ 50 Myr). Once the phase

transition occurs, the bulk of the star formation occurs on time scales much shorter than the dynamical time scale.

3. Results

Figure 1 presents the volume averaged star formation rates for three spheroidal (proto-)galaxies of morphological type E0, E2, and E4. The solid curves represent the average over the inner 1 kpc of a galaxy and the dashed curves correspond to the average over a shell with an inner radius of 7 kpc and an outer radius of 10 kpc.

The initial star formation rate is driven by H_2 cooling, and results in a moderate epoch characterized by a value of the local star formation rate $\sim 10^{-2} \text{ M}_\odot \text{ yr}^{-1}$, due to the dissociation of the H_2 by the stellar radiation field (NS97). The epoch of enhanced star formation starts with the transition to a multi-phase ISM. The three galaxies show a time delay in the star formation peak between the inner and outer region, which is more pronounced for flatter systems. The reason of the delay is the lack of enrichment of the outer regions due to blow-out of metals from the inner regions in the more oblate galaxies. The shoulder on the rising side of the central star formation rates (solid curves) is caused by the rapid increase in metallicity to above the optimal upper limit of $0.1Z_\odot$ in the very inner region on time scales shorter than the bubble propagation time across the entire inner 1 kpc. This gives rise to an enhancement in the magnetic support of the innermost molecular clouds when the ambipolar diffusion time scale becomes longer than the free-fall time. Once the metal-rich hot phase produced during this first burst of star formation has traversed the entire inner 1 kpc and has been mixed with the metal-poor ambient medium, the inner star formation rate reaches its peak. The star formation rates in both the inner and outer regions decrease with decreasing redshift as the available enriched molecular gas decreases because it is converted into stars. One should note that for the galaxy sizes and density

profiles investigated here, no more than 10% of the baryonic mass is in the cold dense phase due to the large energy input of supernova explosions, which heat up the interstellar gas at the star formation peak. For smaller and denser proto-galaxies this percentage increases as the cooling time decreases. Its relation to the early formation of massive ellipticals will be the subject of a follow-up paper.

The massive spherical systems reach their star formation peak in the inner and outer regions as early as $z \sim 4$, whereas more flattened galaxies produce most of their stars between $z = 2.5$ and $z = 1$. This shift is caused by the slower built-up of enriched ISM in the flattened systems, i.e. by the loss of metals through the blow-out phenomenon.

The enriched interstellar gas is a direct measure of the total amount of dust present in the galaxy at any time. For the E0 galaxy, dust-to-gas ratios of 0.01 by mass or more are reached around $z \sim 4$, a value comparable to our own Galaxy. Depending on the actual distribution of the dust, obscuration and depletion of metals into dust grains might occur. The size of this effect is uncertain, and will be discussed elsewhere.

In Figure 2 we show the total volume integrated star formation rate for a sequence of spherical (E0) galaxies of different baryonic masses (and constant baryonic to non-baryonic mass ratio of 0.2; solid curves). The labels “h”, “i” and “l” indicate the high ($5 \times 10^{11} M_{\odot}$), intermediate ($5 \times 10^{10} M_{\odot}$), and low ($\leq 3 \times 10^9 M_{\odot}$) baryonic mass galaxies, respectively. The latter curve is taken from SN97, who study the evolution of dwarf galaxies. These curves indicate that, for a fixed geometry, the formation of stars is delayed to later epochs for lower mass galaxies. Systems with a low binding energy, even though present at high redshifts in hierarchical scenarios of structure formation, do not sustain a multi-phase ISM at those epochs and therefore do not form stars (SN97). Similarly, at constant baryonic mass, the transition to a multi-phase ISM will occur at higher redshifts in systems with larger binding energies. This is illustrated by the dot-dashed curve in Figure 2, which denotes

the intermediate mass E0-i galaxy discussed above, but with a baryonic to non-baryonic mass ratio of 0.04. The very few mass estimates available for star forming systems at high redshift are in agreement with intermediate baryonic masses ($\sim 4 \times 10^{10} M_{\odot}$) embedded in ~ 10 times more massive halos (Warren & Møller 1996). Our results are in good agreement with the idea of “downsizing” with decreasing redshift, as suggested by Cowie et al. (1996) on the basis of their Keck spectroscopy on the Hawaii deep fields.

The dotted curve in Figure 2 depicts the total volume integrated star formation history of the $5 \times 10^{11} M_{\odot}$ proto-galactic disks studied in NS97, i.e. flattened systems with axis ratios smaller than 0.2. These systems are the limiting population of the spheroidal (proto-)galaxies studied in our paper. The massive disks and E0 (proto-)galaxies bracket the redshift dependence of the star formation history caused by geometrical effects. It follows that the flattened systems have had less time by $z = 0$ to form stars and consume their ISM. Our results suggest that the high metal production rate between $z = 1$ and $z = 2$ presented by M96 requires a large fraction of the cosmological star formation to occur at these epochs in flattened and/or low mass systems, and in disks (see also NS97).

It is evident that spheroidal (proto-)galaxies experience a period of star formation which is much shorter when compared to the star formation history of more flattened systems: A large fraction of the baryonic gas is converted into stars within 1 Gyr for roughly spherical, massive (proto-)galaxies. These are in quasi-equilibrium and are dynamically evolving on a free-fall time. Since stars behave as collisionless matter, the rapid conversion of interstellar gas into stars during a quasi-equilibrium collapse phase, might naturally lead to dissipationless collapse and therefore to velocity anisotropies as observed in current epoch elliptical galaxies (van Albada 1982). The final amount of rotational versus anisotropy support will depend on the initial angular momentum of the system and the additional infall of gaseous material. A variety of stellar systems can therefore result. The structure

and stellar populations of the latter will be discussed in a follow-up paper.

4. Discussion and Conclusions

We have shown that massive spherical galaxies can sustain a multi-phase ISM and actively form stars as early as $z \sim 4$. Flatter systems of similar mass reach their peak in star formation and metal production at later epochs due to the blow-out phenomenon, which induces loss of metals in these systems. This provides a natural explanation for the observed galaxy morphologies at high redshifts (G96; S96). The objects observed to form stars at redshifts $z \geq 2$ can be identified with massive, (almost-)round galaxies, or with the inner regions of massive, more flattened systems. These inner regions have a size of the order of the short axis of the galaxies, which regulates the scale length for the occurrence of blow-out, and are comparable to present day bulges. At the same redshifts, the outer regions of flattened galaxies have not yet been significantly enriched. These outskirts are likely to be the nebulosities around many of the compact, spheroidal cores observed in the HDF. The geometrical sequence from round objects to the disks of NS97 also provides a simple explanation for the remarkable “migration” of the sites of intense star formation, from the “bulges” at high- z to the spiral disks at the current epoch (G96). Mergers and possibly dust might be partly responsible for the often observed irregular morphologies at intermediate redshifts. Our models also suggest that massive roundish (proto-)galaxies can sustain star formation as early as $z \sim 4.5$. Relatively few very massive objects with a total mass $M \geq 5 \times 10^{11} M_{\odot}$ will have formed by $z \sim 5$. Still, very red objects are observed at high redshifts (c.f. Dunlop et al. 1996; Dickinson 1996). These might be dust-reddened systems, or the rare relics of the earliest stages of galaxy formation.

Since the peak in dust production coincides with the peak in the star formation rate, massive systems contain large amounts of dust at early epochs. Therefore, a fraction of these

systems might suffer from obscuration. The observations by Omont et al. (1996) of CO 5-4 and CO 7-6 emission toward a radio-quiet quasar at $z = 4.69$ are particularly interesting in this respect. They indicate the presence of a multi-phase ISM with a rich ion-molecule chemistry which requires dust particles for the formation of H_2 and subsequently more complex species. Investigations to assess the importance of the dust obscuration effect will be presented in a future paper, although it has been suggested to be small (M96).

The peak of the metal production rate of the universe, as constrained by currently available observations (M96), occurs at $z \sim 1-2$. This peak coincides with the epochs of star formation of massive proto-galactic disks of NS97 and of low-to-intermediate mass spheroidals. The overall shape of the cosmological star formation rate is obtained by convolving the distribution function, which gives the number of objects of a certain mass and a certain geometry for a given redshift, with the intrinsic star formation histories of galaxies of a certain mass and geometry, and by including the effects of merger-induced star formation not treated here. Future observations with NICMOS and ACS aboard HST promise to further improve our knowledge of the cosmological metal formation history, and possibly unveil substructure related to relatively faint objects such as intermediate-mass spheroidals at their peak of star formation, or flatter systems prior to their star formation peak. A detailed understanding of its redshift dependence, coupled with the results of our models for the mass and geometry of the starforming regions at each epoch, can provide constraints to models of galaxy formation.

We thank Colin Norman, Massimo Stiavelli, and Joe Silk for illuminating discussions. We thank the referee, Max Pettini, for his detailed and stimulating comments. MS acknowledges with gratitude support of NASA grant NAGW-3147 from the Long Term Space Astrophysics Research Program. CMC is supported by NASA through Hubble Fellowship grant HF-1079.01-96a awarded by the Space Telescope Institute, which is

operated by the Association of Universities for Research in Astronomy, Inc., for NASA under contract NAS 5-26555.

REFERENCES

- Cowie, L.L., Songaila, A., & Hu, E.M., 1996, *AJ*, 112, 839
- Cowie, L.L., Hu, E.M., Songaila, A., 1995, *Nature*, 377, 603
- Cole, S., & Lacey, C., 1996, *MNRAS*, 281, 716
- De Young, D.S., & Heckman, T.M., 1994, *ApJ*, 431, 598
- Dickinson, M., 1996, astro-ph/9612178
- Dunlop, J., Peacock, J., Spinrad, H., Dey, A., Jimenez, R., Stern, D., Windhorst, R., 1996, *Nature*, 381, 581
- Fall, S.M., 1996, STScI preprint # 1114
- Fall, S.M., & Pei, Y.C.C., 1993, 402, 479
- Giavalisco, M., Steidel, C.C., Macchetto, F.D., 1996a, *ApJ*, 470, 189 (G96)
- Giavalisco, M., Livio, M., Bohlin, R.C., Macchetto, F.D., Stecher, T.P., 1996b, *AJ*, 112, 369
- Kauffmann, G., 1996, *MNRAS*, 281, 475
- Lacey, C., & Cole, S., 1994, *MNRAS*, 271, 676
- Madau, P., Ferguson, H.C., Dickinson, M.E., Giavalisco, M., Steidel, C.C., & Fruchter, A., 1996, *MNRAS*, 283, 1388 (M96)
- Norman, C.A., & Spaans, M., 1997, *ApJ*, May 1 (NS97)
- Omont, A., Petit-Jean, P., Guilloteau, S., McMahon, R.G., Solomon, P.M., & Pecontal, E., 1996, *Nature*, 382, 428
- Pei, Y.C.C., & Fall, S.M., 1995, 454, 69

Pettini, M., Smith, L.J., Hunstead, R.W., & King, D.L., 1994, *ApJ*, 426, 79

Prochaska, J.X., & Wolfe, A.M., 1997, *ApJ*, 474, 140

Salpeter, E.E., 1955, *ApJ*, 121, 161

Spaans, A., & Norman, C.A., 1997, *ApJ*, July 1 (SN97)

Steidel, C.C., Giavalisco, M., Pettini, M., Dickinson, M.E., & Adelberger, K.L., 1996, *ApJL*, 462, L17 (S96)

van Albada, T.S., 1982, *MNRAS*, 201, 939

Warren, S.J., & Møller, P., 1996, *A&A*, 311, 25

Williams, R.E., et al., 1996, *AJ*, 112, 1335

Fig. 1.— Redshift dependence of the local star formation rate for galaxies of different geometries. The galaxies have a baryonic mass of $5 \times 10^{11} M_{\odot}$ and a radius of $\ell = 15$ kpc. The baryonic to non-baryonic mass ratio is fixed at 0.2. The labels indicate the shape of the galaxy. E0 denotes an axis ratio of unity, E2 of 0.8, and E4 of 0.6. Solid curves represent the inner 1 kpc of the galaxies. The dashed curved correspond to a shell with an inner radius of 7 kpc and an outer radius of 10 kpc.

Fig. 2.— Redshift dependence of the total volume integrated star formation rate for E0 galaxies of different masses. From right to left (solid curves): $5 \times 10^{11} M_{\odot}$ and $\ell = 15$ kpc (E0-h), $5 \times 10^{10} M_{\odot}$ and $\ell = 8$ kpc (E0-i), $\leq 3 \times 10^9 M_{\odot}$ and $\ell \leq 3$ kpc (E0-l). The dotted curve represents the proto-galactic disks of NS97 and the curve for the smallest spheroidals is as computed by SN97. The dashed curve denotes the E0-i model with a baryonic to non-baryonic mass ratio of 0.04 instead of 0.2.

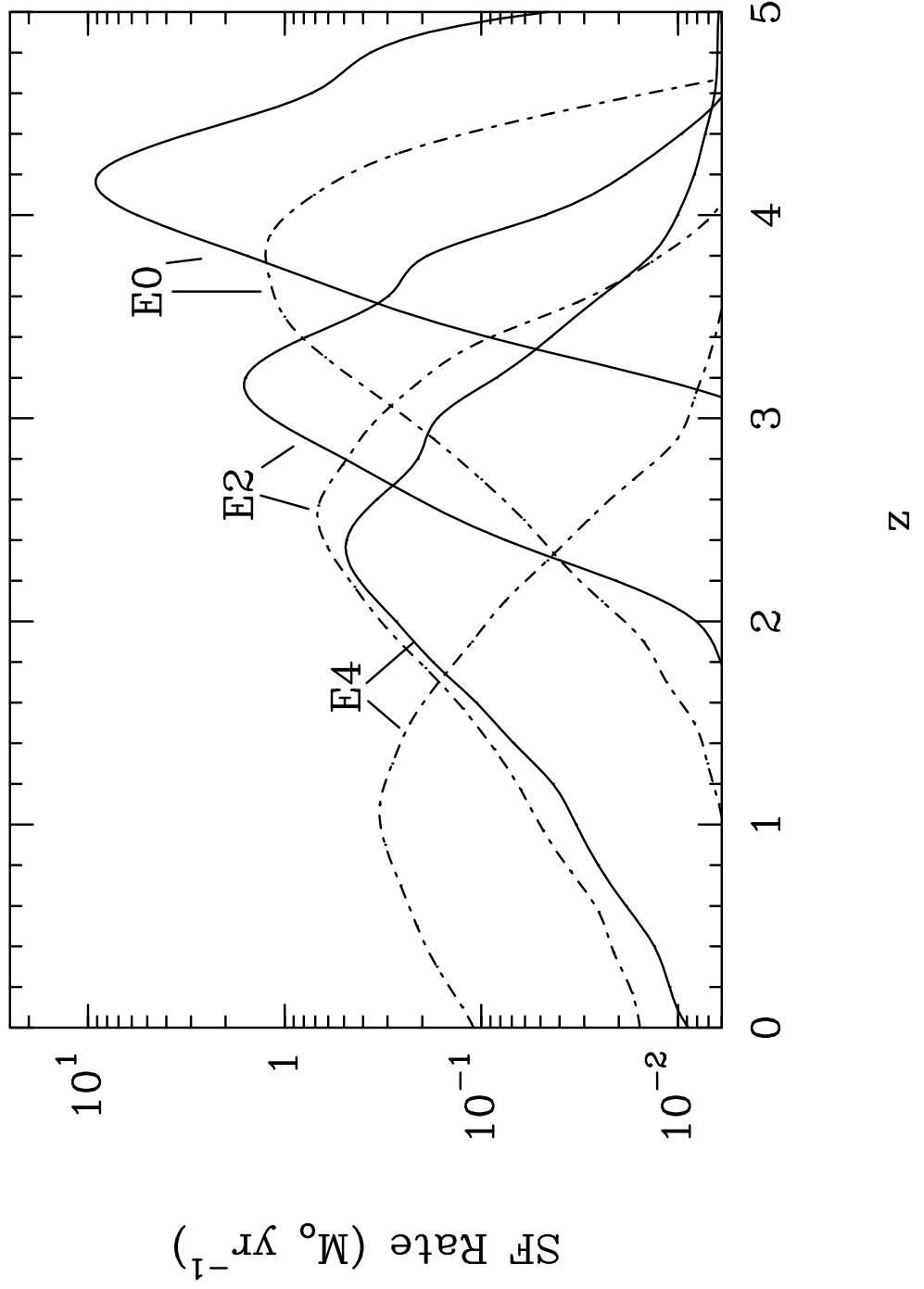


Fig. 1.—

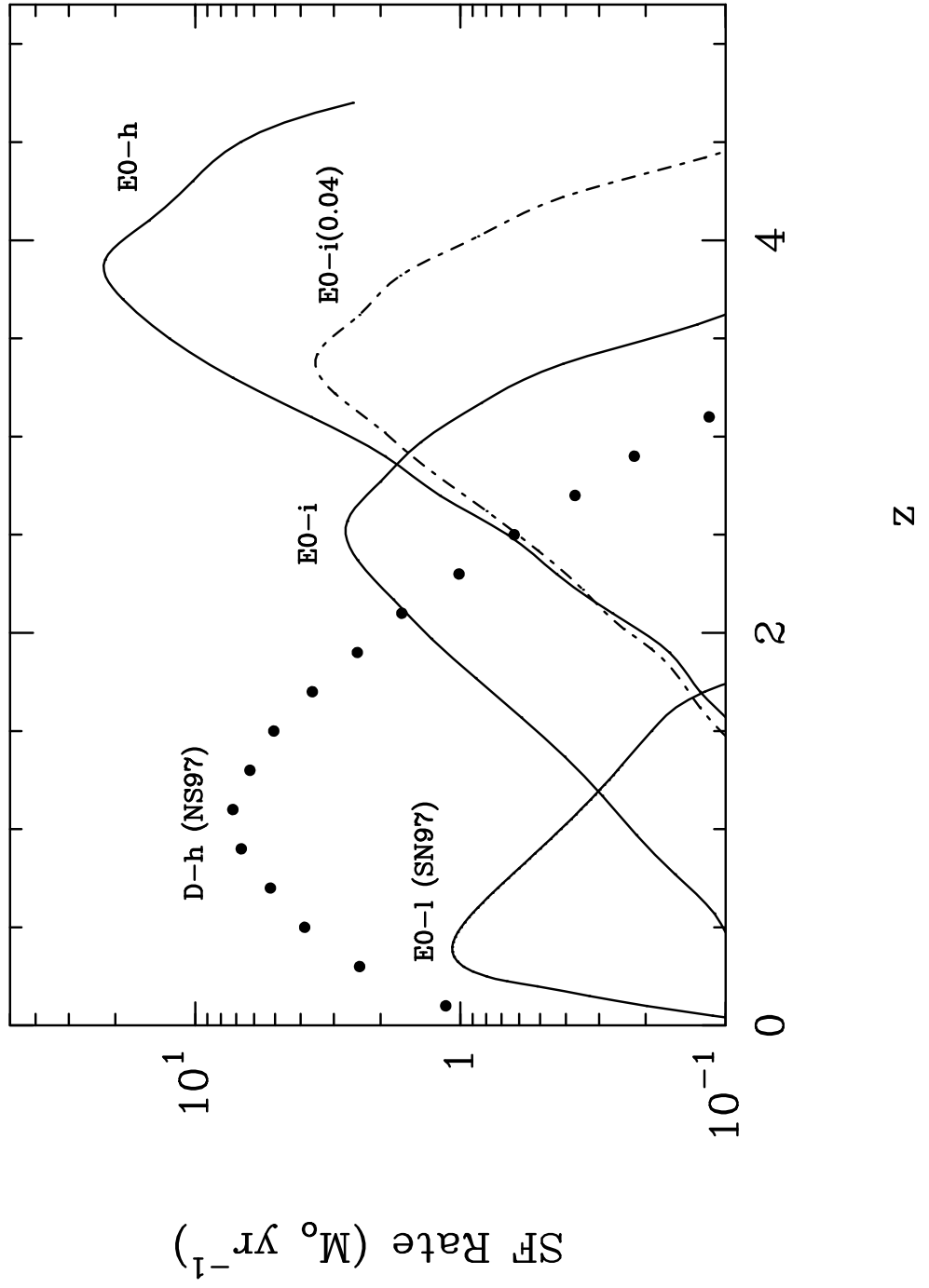


Fig. 2.—